THE CHROMO-WEIBEL INSTABILITY IN AN EXPANDING BACKGROUND*

M. Attems

Frankfurt Institute for Advanced Studies
Ruth-Moufang-Str. 1, 60438 Frankfurt am Main, Germany

A. Rebhan

Institut für Theoretische Physik, Technische Universität Wien
Wiedner Hauptstrasse 8–10, 1040 Vienna, Austria

M. Strickland

Department of Physics, Kent State University, Kent, OH 44242, USA

(Received February 22, 2013)

In this proceedings contribution, we review recent calculations of the dynamics of the chromo-Weibel instability in the quark-gluon plasma. This instability is present in gauge theories which possess a one-particle distribution function which, in the local rest frame, is momentum-space anisotropic. The conditions necessary for triggering this instability can be present already in the color-glass-condensate initial state or dynamically generated by the rapid longitudinal expansion of the matter created in a heavy-ion collision. Using the hard-loop framework, we study the case that the one-particle distribution function possesses an arbitrary initial momentum anisotropy that increases in time due to longitudinal free streaming. The resulting three-dimensional dynamical equations for the chromofield evolution are solved numerically. We find that there is regeneration of the longitudinal pressure due to unstable plasma modes; nevertheless, the system seems to maintain a high-degree of momentum-space anisotropy. Despite this anisotropy, we find that there is rapid longitudinal thermalization of the plasma due to the non-linear mode couplings inherent in the unstable evolution.

DOI:10.5506/APhysPolBSupp.6.393
PACS numbers: 11.15.Bt, 11.10.Wx, 12.38.Mh, 25.75.–q

* Presented by M. Strickland at the International Symposium on Multiparticle Dynamics, Kielce, Poland, September 17–21, 2012.

One outstanding question in the theoretical study of ultrarelativistic heavy ion collisions is the timescale for and processes involved in the thermalization and isotropization of the quark-gluon plasma (QGP). Empirical evidence in favor of fast thermalization and isotropization of the QGP generated in heavy ion collisions was provided by the success of phenomenological relativistic hydrodynamical models [1–9]. The success of these models in describing the collective flow observed at the Relativistic Heavy Ion Collider (RHIC) and the Large Hadron Collider (LHC) suggests that the QGP may become thermal and isotropic on rather short time scales. However, in recent years, there has been an important realization that successful phenomenological application of viscous hydrodynamics may not necessarily imply fast isotropization of the QGP in heavy ion collisions [5, 10–15]. Currently, the question of the degree of momentum-space isotropy of the QGP generated in heavy ion collisions is an open question. In this paper, we review recent numerical calculations [16] which utilize the hard-thermal-loop framework description of an anisotropic QGP.

Due to the rapid longitudinal expansion of the quark-gluon plasma, one expects generation of momentum-space anisotropies in the p_{T}–p_{L} plane. In the weak-coupling limit, the system is expected to be highly-anisotropic at early times. In weakly-coupled quantum chromodynamics (QCD), the presence of momentum-space anisotropies induces unstable plasma modes. The existence and properties of these unstable modes has been studied using kinetic theory and diagrammatic methods [17–27]. This instability has been dubbed the chromo-Weibel instability in reference to the analogous Weibel instability which exists in Abelian electromagnetic plasmas [28]. In the weak-field regime with a fixed momentum-space anisotropy, the chromo-Weibel instability initially causes exponential growth of transverse chromomagnetic and chromoelectric fields; however, due to non-Abelian interaction between the fields, exponentially growing longitudinal chromomagnetic and chromoelectric fields are induced which grow at twice the rate of the transverse field configurations. Eventually, all components of the unstable gauge-field configurations become of equal magnitude. As a result, one finds strong gauge field self-interaction at late times and numerical simulations are necessary in order to have a firm quantitative understanding of the late-time behavior of the system [23, 29–44].

In order to understand the precise role played by the chromo-Weibel instability in ultrarelativistic heavy ion collisions, one must include the effect of the strong longitudinal expansion of the matter. For the first few fm/c of the QGP's lifetime, the longitudinal expansion dominates the transverse expansion. Therefore, to good approximation, one can understand the early time dynamics of the quark-gluon plasma by considering only longitudinal dynamics. The first study to look at the effect of longitudinal

expansion was done in the context of pure Yang–Mills dynamics initialized with color-glass-condensate initial conditions onto which small-amplitude rapidity fluctuations were added [34]. The initial small-amplitude fluctuations result from quantum corrections to the classical dynamics [35, 43, 45]. Numerical studies have shown that adding spatial-rapidity fluctuations results in growth of chromomagnetic and chromoelectric fields with amplitudes $\sim \exp(2m_{\mathrm{D}}^0\sqrt{\tau/Q_{\mathrm{s}}})$, where m_{D}^0 is the initial Debye screening mass and τ is the proper time. This growth with $\exp(\sqrt{\tau})$ was predicted by Arnold *et al.* [23] based on the fact that longitudinal expansion dilutes the density.

In this proceedings contribution, we briefly review our recent paper [16] in which we utilized the hard-expanding-loop framework [46, 47] to numerically determine the evolution of the chromoelectric and chromomagnetic fields induced by fluctuations of a system of high-momentum particles, which are undergoing longitudinal free streaming. Due to the fact that the hard particles are longitudinally free streaming, their local rest frame momentum-space anisotropy $\xi = \frac{1}{2}\langle p_{\mathrm{T}}^2\rangle/\langle p_{\mathrm{L}}^2\rangle - 1$ increases as $\xi = (\tau/\tau_{\mathrm{iso}})^2 - 1$, where τ_{iso} is the proper time at which the distribution function is assumed to be isotropic. In Fig. 1, we plot the unstable mode growth rate Γ/m_{D} for fixed ξ as a function of k_z/m_{D}, where m_{D} is the Debye mass at the proper time τ_{iso}. As can be seen from this figure, as the degree of momentum-space anisotropy increases, more and more modes become unstable. Therefore, when one has a momentum-space anisotropy which is increasing in time, more and more modes become unstable as time progresses. In fact, one finds that at late times $k_{z,\mathrm{max}} \sim m_{\mathrm{D}}\sqrt{\tau/\tau_{\mathrm{iso}}}$, where $k_{z,\mathrm{max}}$ is the wavenumber of the highest mode which is unstable. However, because of the dilution of the particle density due to the longitudinal free streaming, one finds that the maximal

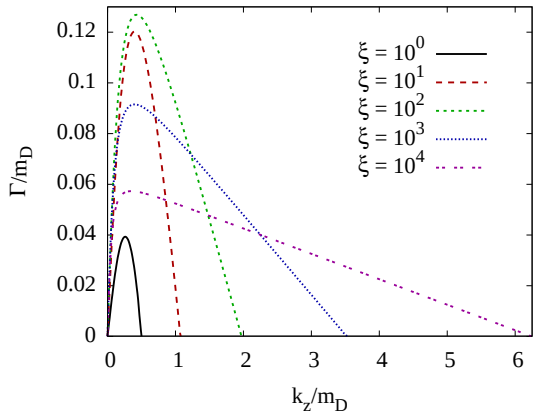

Fig. 1. Unstable mode growth rate Γ/m_{D} for fixed ξ as a function of k_z/m_{D}, where m_{D} is the Debye mass at the proper time τ_{iso}.

unstable growth rate decreases with time as $\Gamma^* \sim m_{\rm D}\sqrt{\tau_{\rm iso}/\tau}$. These two effects compete with one another, with the former causing unstable growth at higher and higher wave numbers as time progresses and the later causing the late time growth to change from a pure exponential to exp $\left(2m_{\rm D}\sqrt{\tau\tau_{\rm iso}}\right)$. Both effects should be taken into account by the dynamical framework for chromofield evolution.

1. Dynamical framework

We assume that the background particles are longitudinally free streaming and, as a result, the background (hard) particles possess a local rest frame momentum-space anisotropy which increases monotonically in proper-time as specified above. Given an isotropic distribution $f_{\rm iso}$, the corresponding free-streaming distribution is

$$f_0(\boldsymbol{p},x) = f_{\rm iso}\left(\sqrt{p_\perp^2 + (p'^z\tau/\tau_{\rm iso})^2}\right) = f_{\rm iso}\left(\sqrt{p_\perp^2 + p_\eta^2/\tau_{\rm iso}^2}\right).$$

Following [46], we obtain the dynamical equation obeyed by color perturbations δf^a of a color-neutral longitudinally free-streaming momenta distribution f_0 which can be written compactly as

$$V\cdot D\,\delta f^a|_{p^\mu} = gV^\mu F^a_{\mu\nu}\partial^\nu_{(p)} f_0(\boldsymbol{p}_\perp, p_\eta)\,.$$

This equation must be solved simultaneously with the non-Abelian Yang–Mills equations which couple the color-charge fluctuations back to the gauge fields via the induced color-currents j^ν_a

$$D_\mu F^{\mu\nu}_a = j^\nu_a = g\,t_R\int\frac{d^3p}{(2\pi)^3}\frac{p^\mu}{2p^0}\delta f_a(\boldsymbol{p},\boldsymbol{x},t)\,, \tag{1}$$

where $D_\alpha = \partial_\alpha - ig[A_\alpha,\cdot]$ is the gauge covariant derivative and $F_{\alpha\beta} = \partial_\alpha A_\beta - \partial_\beta A_\alpha - ig[A_\alpha, A_\beta]$ is the field strength tensor, and g is the strong coupling. The above equations are then transformed to comoving coordinates with the metric $ds^2 = d\tau^2 - d\boldsymbol{x}_\perp^2 - \tau^2 d\eta^2$.

The resulting dynamical equations are numerically solved in temporal axial gauge on a spatial lattice. In order to maintain gauge invariance with respect to three-dimensional gauge transformations, the spatially-discretized fields are represented by plaquette variables and evolved along with the conjugate momentum using a leap-frog algorithm. The fluctuation-induced currents are represented by auxiliary fields which are discretized in space and also on a cylindrical velocity-surface spanned by azimuthal velocity and rapidity. As a result, the simulations are effectively five-dimensional and are, therefore, computationally intensive. For details concerning the numerical implementation, we refer the reader to Ref. [16].

2. Results

We used a five-dimensional lattice size of $(N_\perp^2 \times N_\eta) \times (N_u \times N_\phi) = (40^2 \times 128) \times (128 \times 32)$ with transverse spatial lattice spacing of $a = Q_s^{-1}$ and longitudinal spatial lattice spacing of $a_\eta = 0.025$. Here, Q_s is the nuclear saturation scale which is approximately 2 GeV and 1.4 GeV at LHC and RHIC energies, respectively. For the initial conditions, we seeded current fluctuations of amplitude Δ which had a UV spectral cutoff (see Ref. [16] for details of the spectrum of initial fluctuations). In Fig. 2 (left), we show the various components of the chromofield energy density as a function of rescaled proper time $\tilde{\tau}$. For LHC and RHIC initial energy densities, one unit in $\tilde{\tau}$ corresponds to approximately 1 fm/c and 1.4 fm/c, respectively. For this figure, an initial fluctuation amplitude of $\Delta = 0.8$ was chosen. As can be seen from this figure, after approximately 1 fm/c, we begin to see rapid growth of the transverse chromomagetic field, followed by the transverse chromoelectric field, and then the longitudinal chromofields. In Fig. 2 (right), we show the resulting ratio of the total (particle plus field) longitudinal pressure divided by the total transverse pressure for various values of Δ. At early times, prior to unstable mode growth, one observes from this figure that the longitudinal pressure drops due to the longitudinal free streaming of the hard particle background; however, when the unstable modes begin to grow, one observes a regeneration of the longitudinal pressure by the unstable modes which have their wave vectors pointed primarily along the longitudinal direction. In addition, one observes that the time at which isotropy is restored is primarily sensitive to the initial fluctuation amplitude Δ.

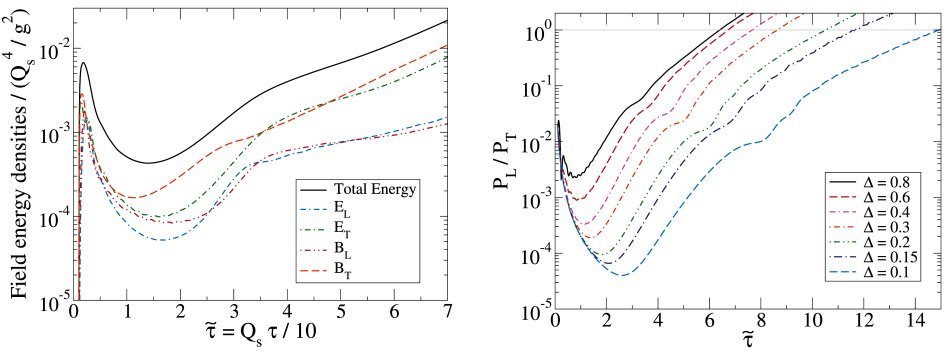

Fig. 2. On the left, we plot the various components of the chromofield energy density as a function of proper time. On the right, we plot of the total (field plus particle) longitudinal over transverse pressure as a function of proper time.

In addition to extracting information about the energy density and pressures of the system as a function of proper time, one can also extract information from the gauge field spectra. The longitudinal spectra can be

obtained following Ref. [45] by first Fourier transforming each field component $E_\perp(x_\perp,\eta)$, $E_\eta(x_\perp,\eta)$, $B_\perp(x_\perp,\eta)$ and $B_\eta(x_\perp,\eta)$, integrating over the transverse wave vectors and decomposing each according to the longitudinal wave vector ν, in terms of which the electric and magnetic energy densities are decomposed into longitudinal energy spectra (see Ref. [16] for details). One problem with such spectra is that they are not gauge invariant. As an additional spectral measure, we also extract the transverse momentum-averaged longitudinal spectra obtained by Fourier-transforming the spatial distribution of the total field energy density. In Fig. 3 (left), we show the extracted longitudinal spectra extracted using the first method averaged over 50 runs. The spectra extracted using the second method have similar features to the left panel but, due to limited space, we do not show them here (see the left panel of Fig. 4 in Ref. [48] for this plot). In Fig. 3 (right), we plot the gauge-field temperature extracted from the spectra via fits to the form $\mathcal{E} \propto \int dk_z \left(k_z^2 + 2|k_z|T + 2T^2\right) \exp\left(-|k_z|/T\right)$ which is obtained by integrating a Boltzmann distribution over transverse momenta. In the figure, we show the fitted temperature obtained from both types of extracted spectra (the first method is indicated as '$T_{\rm L}$' and the second method as '$T_{\rm L}$ $(\overline{\mathcal{E}})$'). In both cases, one sees that after an initial period of cooling, the gauge sector begins to heat up with the temperatures extracted using the two methods being approximately the same. We note that the quality of the fits is extremely good (see Fig. 10 of Ref. [16] for comparisons of the fitted function to the data at various proper times). The fit function above begins to describe the observed spectra very well at early times corresponding to $\tilde{\tau} \sim 1$ indicating extremely fast longitudinal thermalization of the spectra even though the system is still highly anisotropic at this moment in time.

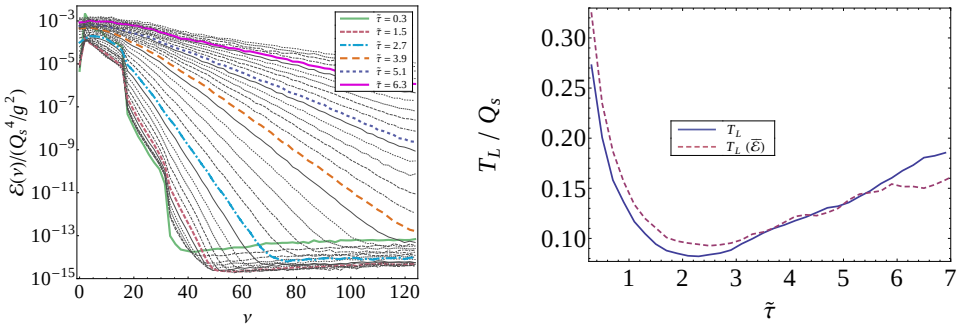

Fig. 3. On the left, we plot the longitudinal spectra at various proper times. On the right, we plot the extracted longitudinal temperature which was obtained by a fit (see the text) to the longitudinal spectra ($\mathcal{E}$) or the Fourier-transform of the spatial energy density ($\overline{\mathcal{E}}$).

3. Conclusions

In this proceedings contribution, we have briefly reviewed the recent findings of our three-dimensional hard-expanding-loop simulations. The chief results were: *(i)* one sees regeneration of the longitudinal pressure by unstable chromofield modes, however, the system remains anisotropic for many fm/c; *(ii)* despite being anisotropic, there appears to be a rapid longitudinal thermalization due to non-linear mode couplings induced by unstable mode growth. In the future, we are planning to improve our numerical results by utilizing much larger lattice sizes and also studying pure Yang–Mills dynamics in an expanding metric.

M.A. acknowledges funding of the Helmholtz Young Investigator Group VH-NG-822. M.S. was supported by NSF grant No. PHY-1068765.

REFERENCES

[1] P. Huovinen *et al.*, *Phys. Lett.* **B503**, 58 (2001) [arXiv:hep-ph/0101136].

[2] T. Hirano, K. Tsuda, *Phys. Rev.* **C66**, 054905 (2002) [arXiv:nucl-th/0205043].

[3] A. Muronga, *Phys. Rev. Lett.* **88**, 062302 (2002) [arXiv:nucl-th/0104064].

[4] K. Dusling, D. Teaney, *Phys. Rev.* **C77**, 034905 (2008) [arXiv:0710.5932 [nucl-th]].

[5] M. Luzum, P. Romatschke, *Phys. Rev.* **C78**, 034915 (2008) [arXiv:0804.4015 [nucl-th]].

[6] B. Schenke, S. Jeon, C. Gale, *Phys. Lett.* **B702**, 59 (2011) [arXiv:1102.0575 [hep-ph]].

[7] C. Shen *et al.*, *Phys. Rev.* **C84**, 044903 (2011) [arXiv:1105.3226 [nucl-th]].

[8] H. Niemi *et al.*, *Phys. Rev.* **C86**, 014909 (2012) [arXiv:1203.2452 [nucl-th]].

[9] P. Bozek, I. Wyskiel-Piekarska, *Phys. Rev.* **C85**, 064915 (2012) [arXiv:1203.6513 [nucl-th]].

[10] M. Martinez, M. Strickland, *Phys. Rev.* **C78**, 034917 (2008) [arXiv:0805.4552 [hep-ph]].

[11] H. Song, arXiv:0908.3656 [nucl-th].

[12] P.M. Chesler, L.G. Yaffe, *Phys. Rev. Lett.* **106**, 021601 (2011) [arXiv:1011.3562 [hep-th]].

[13] M.P. Heller, R.A. Janik, P. Witaszczyk, *Phys. Rev.* **D85**, 126002 (2012) [arXiv:1203.0755 [hep-th]].

[14] M. Martinez, R. Ryblewski, M. Strickland, *Phys. Rev.* **C85**, 064913 (2012) [arXiv:1204.1473 [nucl-th]].

[15] R. Ryblewski, W. Florkowski, *Phys. Rev.* **C85**, 064901 (2012) [arXiv:1204.2624 [nucl-th]].

[16] M. Attems, A. Rebhan, M. Strickland, *Phys. Rev.* **D87**, 025010 (2013) [arXiv:1207.5795 [hep-ph]].

[17] U.W. Heinz, *Nucl. Phys.* **A418**, 603C (1984).

[18] Y. Pokrovsky, A. Selikhov, *JETP Lett.* **47**, 12 (1988).

[19] S. Mrowczynski, *Phys. Lett.* **B314**, 118 (1993).

[20] S. Mrowczynski, M.H. Thoma, *Phys. Rev.* **D62**, 036011 (2000) [arXiv:hep-ph/0001164].

[21] J. Randrup, S. Mrowczynski, *Phys. Rev.* **C68**, 034909 (2003) [arXiv:nucl-th/0303021].

[22] P. Romatschke, M. Strickland, *Phys. Rev.* **D68**, 036004 (2003).

[23] P.B. Arnold, J. Lenaghan, G.D. Moore, *J. High Energy Phys.* **0308**, 002 (2003) [arXiv:hep-ph/0307325]; *Erratum* added online, September 29, 2004.

[24] S. Mrowczynski, A. Rebhan, M. Strickland, *Phys. Rev.* **D70**, 025004 (2004) [arXiv:hep-ph/0403256].

[25] P.B. Arnold, J. Lenaghan, *Phys. Rev.* **D70**, 114007 (2004) [arXiv:hep-ph/0408052].

[26] P. Romatschke, M. Strickland, *Phys. Rev.* **D70**, 116006 (2004) [arXiv:hep-ph/0406188].

[27] P.B. Arnold *et al.*, *Phys. Rev. Lett.* **94**, 072302 (2005) [arXiv:nucl-th/0409068].

[28] E.S. Weibel, *Phys. Rev. Lett.* **2**, 83 (1959).

[29] A. Rebhan, P. Romatschke, M. Strickland, *Phys. Rev. Lett.* **94**, 102303 (2005) [arXiv:hep-ph/0412016].

[30] P.B. Arnold, G.D. Moore, L.G. Yaffe, *Phys. Rev.* **D72**, 054003 (2005) [arXiv:hep-ph/0505212].

[31] A. Rebhan, P. Romatschke, M. Strickland, *J. High Energy Phys.* **0509**, 041 (2005) [arXiv:hep-ph/0505261].

[32] P.B. Arnold, G.D. Moore, *Phys. Rev.* **D73**, 025006 (2006) [arXiv:hep-ph/0509206].

[33] P.B. Arnold, G.D. Moore, *Phys. Rev.* **D73**, 025013 (2006) [arXiv:hep-ph/0509226].

[34] P. Romatschke, R. Venugopalan, *Phys. Rev.* **D74**, 045011 (2006) [arXiv:hep-ph/0605045].

[35] K. Fukushima, F. Gelis, L. McLerran, *Nucl. Phys.* **A786**, 107 (2007) [arXiv:hep-ph/0610416].

[36] D. Bodeker, K. Rummukainen, *J. High Energy Phys.* **0707**, 022 (2007) [arXiv:0705.0180 [hep-ph]].

[37] P.B. Arnold, G.D. Moore, *Phys. Rev.* **D76**, 045009 (2007) [arXiv:0706.0490 [hep-ph]].

[38] J. Berges, S. Scheffler, D. Sexty, *Phys. Rev.* **D77**, 034504 (2008) [arXiv:0712.3514 [hep-ph]].

[39] J. Berges, S. Scheffler, D. Sexty, *Phys. Lett.* **B681**, 362 (2009) [arXiv:0811.4293 [hep-ph]].

[40] J. Berges *et al.*, *Phys. Lett.* **B677**, 210 (2009) [arXiv:0812.3859 [hep-ph]].

[41] J. Berges, J. Pruschke, A. Rothkopf, *Phys. Rev.* **D80**, 023522 (2009) [arXiv:0904.3073 [hep-ph]].

[42] A. Ipp, A. Rebhan, M. Strickland, *Phys. Rev.* **D84**, 056003 (2011) [arXiv:1012.0298 [hep-ph]].

[43] K. Dusling, F. Gelis, R. Venugopalan, *Nucl. Phys.* **A872**, 161 (2011) [arXiv:1106.3927 [nucl-th]].

[44] J. Berges, K. Boguslavski, S. Schlichting, *Phys. Rev.* **D85**, 076005 (2012) [arXiv:1201.3582 [hep-ph]].

[45] K. Fukushima, F. Gelis, *Nucl. Phys.* **A874**, 108 (2012) [arXiv:1106.1396 [hep-ph]].

[46] P. Romatschke, A. Rebhan, *Phys. Rev. Lett.* **97**, 252301 (2006) [arXiv:hep-ph/0605064].

[47] A. Rebhan, M. Strickland, M. Attems, *Phys. Rev.* **D78**, 045023 (2008) [arXiv:0802.1714 [hep-ph]].

[48] M. Attems, A. Rebhan, M. Strickland, arXiv:1301.7749 [hep-ph].